# Incorporating Surface Soil Moisture Information in Error Modeling of TRMM Passive Microwave Rainfall

Hojjat Seyyedi, Emmanouil N. Anagnostou, Pierre-Emmanuel Kirstetter, Viviana Maggioni, Yang Hong, and Jonathan J. Gourley

***Abstract*—This study assesses the significance of conditioning the error modeling of The National Aeronautics and Space Administration (NASA)'s Tropical Rainfall Measurement Mission Microwave Imager rainfall algorithm (2A12) to near-surface soil moisture data derived from a land surface model. The term "conditioning" means the model parameters' dependence on soil wetness. The Oklahoma (OK) region is used as the study area due to its relatively low vegetation and smooth terrain and the availability of high-quality *in situ* hydrometeorological data from the Mesonet network. The study period includes two warm seasons (March to October) from 2009 and 2010. The National Oceanic and Atmospheric Administration/National Severe Storms Laboratory ground radar-based National Mosaic and Quantitative Precipitation Estimation system (NMQ/Q2) is used as high-resolution (5-min/1-km) reference rainfall. The surface wetness conditions (wet, dry, and normal) were determined from surface soil moisture fields simulated by the NASA Catchment Land Surface Model forced with Q2 rainfall fields. A 2-D satellite rainfall error model, SREM2D, is used to provide the ensemble error representation of 2A12 rainfall using two different parameter calibration approaches: conditioning the SREM2D parameters to the surface soil wetness categories versus not. The statistical analysis of model-generated ensembles and associated error metrics show better performance when surface wetness information is used in SREM2D. In terms of quantification, the ensemble rainfall from the conditional SREM2D parameter calibration shows better reference rainfall encapsulation. The conditioning of SREM2D to soil wetness can apply to rainfall rate estimates from other microwave sensors on board low Earth orbiting satellites and is valuable for the forthcoming missions on precipitation (Global Precipitation Measurement) and soil moisture (Soil Moisture Active Passive).**

Manuscript received May 7, 2013; revised September 14, 2013 and November 12, 2013; accepted November 25, 2013. This work was supported in part by the NASA Precipitation Science Team Grant NNX07AE31G and in part by NASA Precipitation Measurement Mission Award NNX13AF72G.

H. Seyyedi and E. N. Anagnostou are with the Department of Civil and Environmental Engineering, University of Connecticut, Storrs, CT 06269-3037 USA (e-mail: manos@engr.uconn.edu).

P.-E. Kirstetter is with the School of Civil Engineering and Environmental Sciences, University of Oklahoma, Norman, OK 73019-1024 USA. He is also with the NOAA/National Severe Storms Laboratory, Norman, OK 73072 USA, and also with the Advanced Radar Research Center, National Weather Center, Norman, OK 73072 USA.

V. Maggioni is with the Department of Civil, Environmental, and Infrastructure Engineering at George Mason University, Fairfax, VA 22030 USA.

Y. Hong is with the School of Civil Engineering and Environmental Sciences, University of Oklahoma, Norman, OK 73019-1024 USA.

J. J. Gourley is with the NOAA/National Severe Storms Laboratory, Norman, OK 73072 USA, and also with the Advanced Radar Research Center, National Weather Center, Norman, OK 73072 USA.

Color versions of one or more of the figures in this paper are available online at http://ieeexplore.ieee.org.

Digital Object Identifier 10.1109/TGRS.2013.2295795

***Index Terms*—Error modeling, quantitative precipitation estimation (QPE), satellite, soil moisture.**

## I. Introduction

THE critical role of precipitation on hydrological processes requires accurate estimates over land at the highest possible spatiotemporal resolution. The conventional ground-based rainfall measurements exhibit significant limitations as well as error sources. Specifically, measurements from rain gauges and weather radars are associated with sampling issues due to the uneven distribution of sensors and limited spatial coverage. As a consequence, time and coverage gaps, particularly over complex terrain and several developing regions of the globe, limit the representativeness of those measurements in hydrologic modeling [1]. Scientists have also raised inquiries for radar measurements due to issues with radar calibration, variability in reflectivity-to-rainfall transformation, beam geometry, and precipitation profile effects, among others [2]–[4].

Since the 1970s, meteorological satellites have been operational, providing valuable remote-sensing observations of rainfall over remote and ungauged regions of the Earth [5]. Depending on the type, i.e., geostationary versus low Earth orbit, it can carry the range of visible, infrared, and microwave sensors [6]–[8]. Passive microwave (PMW) frequencies have been used for rain retrieval from low Earth orbiting sensors for about 25 years. The techniques that have been developed and refined in time rely on the signal emitted by raindrops over oceans at frequencies at or below 37 GHz and on the scattering signal of ice particles in the precipitation layer over land at frequencies at or above 85 GHz [9]. Depending on the type of satellite sensor and designated goals, different PMW precipitation retrieval algorithms have been developed. Each product has its own strengths and weaknesses, but none of them appears to be universally better than the other [10]. A widely used algorithm for precipitation retrieval from PMW frequencies is the Goddard Profiling (GPROF) technique [11], [12]. GPROF is a Bayesian based approach to retrieve the instantaneous rainfall with matching observed and simulated brightness temperature databases through a radiative transfer model. Despite the sturdy linkage of PMW precipitation retrieval algorithms with the physical processes of precipitation formation, GPROF exhibits acceptable performances in heavy rain convective conditions over the ocean. However, over land surface, Lensky and

Levizzani [9] have indicated that PMW retrieval algorithms are suffering from uncertainties in precipitation-type classification and temporal resolution.

The precipitation radar (PR) on board the Tropical Rainfall Measuring Mission (TRMM) satellite that samples the vertical profile of precipitation can provide higher accuracy measurements against other space-based products, and to this capacity, it contributes on evaluating and developing PMW retrieval algorithms, such as the TRMM Microwave Imager (TMI—hereafter named 2A12) overland rain estimation algorithm [13]–[15]. 2A12 has different rainfall retrieval procedures for each surface type (ocean, land, and coastal regions) to account for differences in the microwave emission characteristics. Rainfall has high emissivity and is nonpolarized at PMW frequencies, which makes it possible to distinguish it from the ocean surface that is associated with low emissivity and high polarization. The overland retrieval algorithm faces more complexity due to the land cover changes and variable emissivity surface background, aside from the nonpolarized nature of the land [12], [16], and it is affected by a large number of surface parameters such as soil moisture, vegetation properties, and snow cover [17]. Due to the surface complexity, the 85-GHz brightness temperature (Tb) observations associated with ice scattering have been the primary data for overland rainfall estimation. However, a screening procedure is required for PMW overland rainfall retrievals to define rain versus no-rain areas and to mask out regions producing scattering signals similar to rainfall, such as deserts, semiarid land, and snow cover [18].

The 2A12 algorithm has been extensively evaluated over land through comparisons with ground-based gauges and radar rainfall data, aircraft measurements, and other spaceborne products [12], [19], [20]. Several deficits associated with the 2A12 land algorithm have been identified and discussed in those studies. Overall, the algorithm tends to overestimate rainfall rates from convective systems and to underestimate the rainfall that resulted from the droplet coalescence processes and warm rainfall due to the lack of 85-GHz depression [12], [20]–[22]. The sensitivity of the rain screening algorithm to snow background and deserts enhances false alarms of the algorithm over those regions [12], [23]. Recently, Kirstetter *et al.* [24] presented the joint influence of precipitation structure and surface conditions (soil wetness and vegetation cover) on the error structure of the 2A12 product over land. While more research is needed to quantify the impact of specific factors like precipitation horizontal and vertical structure or vegetation water content, the biases of the 2A12 algorithm appear to be significantly organized alongside the surface wetness. Specifically, 2A12 is shown to overestimate under both dry and wet conditions, with stronger overestimation exhibited under dry surface conditions. The authors attributed the associated overestimation of 2A12 to biases in the convective precipitation fraction classification, which were shown to be sensitive to surface wetness conditions.

Anomalies associated with 2A12 show underestimation in warm rain and overestimation in deep convective events. This plays an indubitable role in water resources management and hydropower system operation as a part of satellite rainfall product application. Thus, improving the accuracy and the error characterization of 2A12 rainfall estimates is critical for a number of satellite rainfall products and applications [12], as uncertainties in the 2A12 algorithm propagate to TRMM-based global multisatellite rainfall estimates.

After having identified potential (physical) error factors, their impact on satellite rainfall uncertainties needs to be quantified. An empirical way to assess this impact is simulating error-corrected rainfall fields while accounting, or not, for the error factor at stake. Hossain and Anagnostou [25] have developed a multidimensional satellite rainfall error model (SREM2D), which has been used in several studies to produce ensemble rainfall fields representing realizations of error-adjusted satellite rainfall products [26]–[28]. Triggered by the Kirstetter *et al.* [24] preliminary findings on soil wetness effects in TMI rainfall, this paper aims to quantify the impact of accounting for soil wetness in the statistical error modeling of 2A12 rainfall retrieval through SREM2D.

The surface soil moisture condition was determined in this study from NASA's Community Land Surface Model simulations and used to derive area-averaged volumetric soil moisture values within 2A12's orbit over Oklahoma. Overpasses associated with less (more) than the 25th (75th) quantile of the cumulative distribution are considered as dry (wet) conditions, whereas the remaining overpasses constitute normal wetness conditions. SREM2D parameters are calculated with and without considering the aforementioned orbit-average surface soil moisture classification. It is often convenient to separate the error in two components: the systematic error and the random error. The significance of accounting for soil wetness will be assessed by quantifying its impact on the average discrepancies between the rainfall ensemble and the reference (systematic error) as well as on the spread of the ensemble (random error). The systematic and random error quantification of simulated referencelike ensemble members will indicate the significance of considering the area-average surface soil wetness condition in the error modeling of 2A12.

In the next section, we present the study area and data sets. In Section III, we describe the 2A12 rainfall error analysis, and in Section IV, we describe the SREM2D and the parameter calibration, which is performed accounting—and not—for the soil wetness conditioning term. Finally, Section V presents the results and major findings from this research.

## II. Study Area and Data

The study area is located in Oklahoma (OK) in the south-central United States (ranging from 32N to 39N and 93W to 102W; see Fig. 1). The region has an elevation gradient from west to southeast, with the highest peak in the northwestern corner and the lowest point in the southeastern corner, respectively, with 1515 and 88 m above sea level. The study area is located in the tepid latitude of the globe, where cold and warm fronts interact frequently, yielding severe events and laying the region on the Tornado Alley. The high spatial gradient of soil moisture across the region makes it an ideal test bed for studying the sensitivity of the rainfall retrievals for various soil moisture conditions. Established networks of *in situ* sensors from the Oklahoma Mesonet and the good radar coverage from the next-generation radar (NEXRAD) network provide

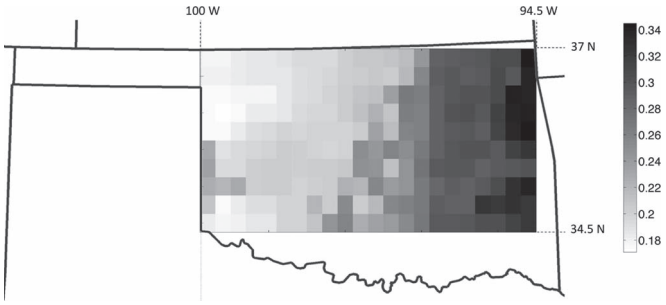


Fig. 1. Map of seven-year (2004–2010) average surface soil moisture $(\mathrm{m}^3/\mathrm{m}^3)$ simulated by CLSM, overlaid by the 25-km grid of the study domain.

high-resolution information on the land-surface state and on the rainfall in the Oklahoma region. The Q2-based radar rainfall, 2A12 rainfall estimates, and soil moisture simulations from the NASA Catchment Land Surface Model (CLSM) utilized in this study are described next.

### A. Q2 Radar-Based Reference Rainfall

All significant rain fields observed coincidentally by TRMM overpasses and the NEXRAD (http://www.roc.noaa.gov/WSR88D/) radar network over the study area from March to October of 2009 and 2010 are collected. The National Oceanic and Atmospheric Administration/National Severe Storms Laboratory National Mosaic and Quantitative Precipitation Estimation system (named Q2; see [29]) combines information from all ground-based radars comprising the Weather Surveillance Radar-1988 Doppler network (NEXRAD) to derive experimental radar-based products comprising high-resolution (0.01°, 5 min) instantaneous rainfall rate mosaics available over the Continental United States [30]–[33].

Many errors affect the estimation of rainfall from ground-based radars, such as nonweather echoes, nonuniform beam filling, range dependence due to vertical profile of reflectivity (VPR) variability, conversion of Z to R, and calibration of the radar signal (see [34] for a review). While several procedures are already in place within the Q2 system to correct for these errors, additional postprocessing steps were taken to refine the reference data set as much as possible.

The original Q2 products utilized in this study are as follows: 1) the radar-only instantaneous rain rate (RR) national mosaic updated every 5 min; 2) the radar-only RR national mosaic at an hourly time step; and 3) the hourly rain gauge-corrected national mosaic product. The reference rainfall is derived from an instantaneous bias-corrected Q2 product. Instantaneous Q2 products are adjusted using colocated rain gauge observations to minimize the aforementioned errors: Pixel-by-pixel ratios between the hourly gauge-adjusted and the hourly radar-only products are calculated and applied as multiplicative adjustment factors to the radar-only 5-min product. This adjustment is designed to minimize uncertainties with the Z–R relationship and calibration errors (see [35] for more details). Extreme adjustment factors (outside the [0.1–10] range) are discarded, so the gauge adjustment also serves as a data quality control procedure. Note that the rain gauge network in Oklahoma is dense and well suited to provide reliable hourly adjustments in the radar rainfall estimates. Moreover, working with data from the summer season over a generally flat terrain avoids overestimation in the bright band and mitigates range dependence caused by VPR effects, so the best measurement conditions (i.e., no beam blockage and radar beam below the melting level of rainfall) are retained. Although the quantitative interpretation of the weather radar signal in terms of rainfall may be complex, radars enable a reliable evaluation of area-averaged rainfall estimates.

The Q2 5-min products that encapsulate the TRMM satellite local overpass schedule time are used as the reference rainfall fields to the corresponding 2A12 rainfall estimates. Specifically, the reference rainfall $R_{\mathrm{ref}}$ is computed from a block-Q2 rainfall pixel matching each land surface model pixel. All Q2 pixels (rainy and nonrainy) corresponding to a land surface model pixel are used to compute the pixel-average reference rainfall rate.

### B. TMI 2A12 Rainfall Algorithm

The TMI Level 2 Hydrometeor Profile Product, 2A12 (version 7), with a horizontal resolution of ∼5 km at 85.5 GHz is evaluated in this study. The algorithm is detecting rain versus no-rain areas through establishing a relationship between the RR and the 85- and 21-GHz vertically polarized channels using coincident TMI and TRMM PR data for both convective and stratiform data. Then, the algorithm defines the percentage of convective and stratiform rainfall patterns by calculating the convective probability of observed rainfall while accounting for TB10V, TB37V, TB85V, and TB85H, which are the 10- and 37-GHz vertically and 85-GHz vertically (horizontally) polarized channels, respectively [15], [16]. The convective/stratiform pattern recognition reduces the associated uncertainty with possible rainfall rates for a given brightness temperature. Kirstetter *et al.* [24] performed a diagnostic error characterization on 2A12 rainfall estimates conditioned by the surface wetness, cloud structure, and vegetation covers. During summer, better satellite performance was reported over regions with wetter soil moisture conditions. Regarding rainfall detection, the missed rain volume was shown to decrease for increasing surface wetness conditions. In terms of quantification, the 2A12 algorithm exhibited a greater overestimation (up to 55%) over dry surface conditions and a lower one (less than 10%) over wet surface conditions. This was attributed to overestimation in the convective rain fraction, which was shown to increase inverse proportionally to soil wetness. Therefore, soil moisture is identified as a potential factor for the 2A12 rainfall retrieval error, which will be modeled in Section III using SREM2D.

### C. Simulations of Surface Soil Moisture

Surface conditions were assessed through surface soil moisture estimates from the NASA CLSM [36], [37]. This model uses a catchment-based method to assess land surface processes, as the hydrological catchment defined by topography is the essential element of the land surface model. The variability of soil moisture is associated with three bulk soil moisture variables at the element scale. These variables display equilibrium conditions and nonequilibrium conditions. In particular, equilibrium conditions are associated with the water table

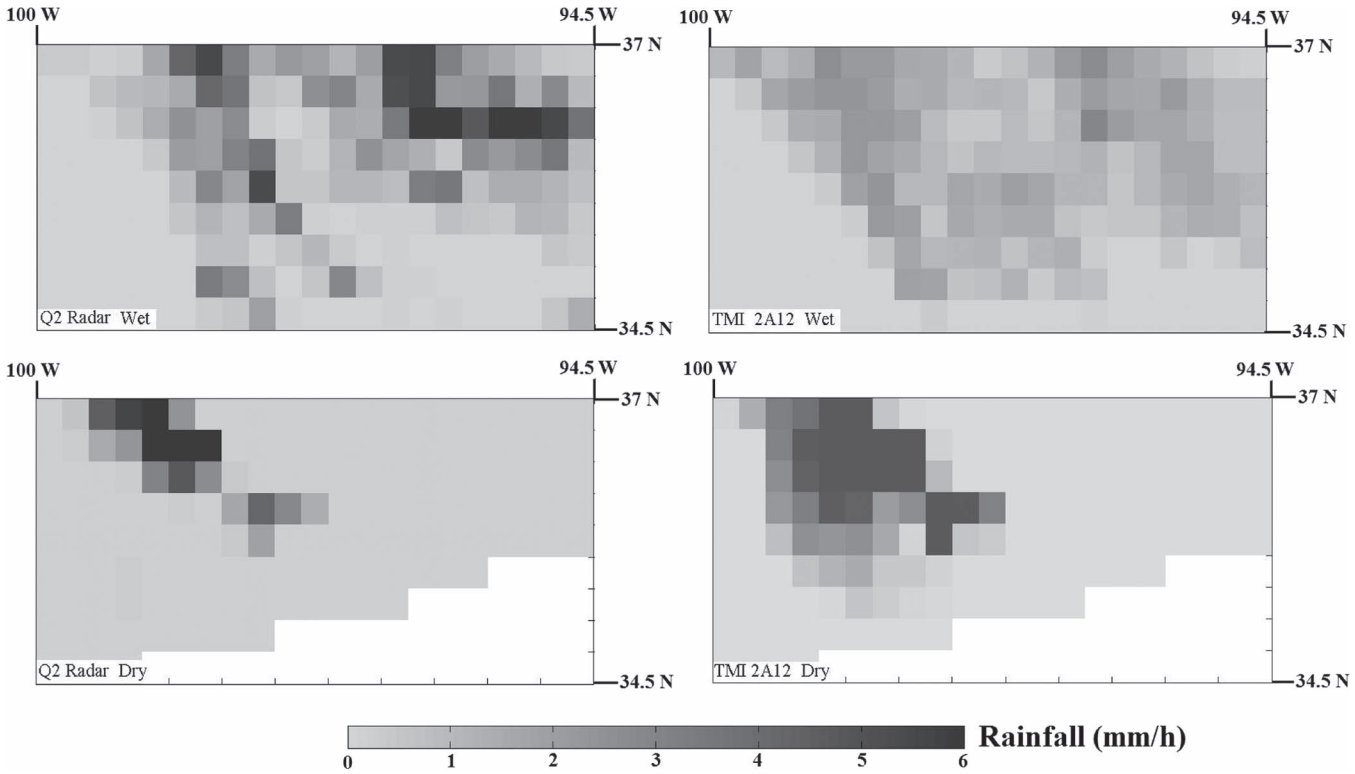


Fig. 2. Precipitation maps from 2a12 and Q2 radar. (a) Wet soil condition, September 12, 2009, 21:45 h (top). (b) Dry soil condition, July 17, 2009, 03:55 h (bottom). Dashed lines indicate the 2A12 orbit over the study domain.

distribution, and nonequilibrium conditions are found near the land surface.

CLMS utilizes several surface level meteorological variables (precipitation, air temperature, and radiation, among others) and predetermined climatological vegetation parameters. CLMS is forced with precipitation data from the bias-corrected Q2-based rainfall data set, and the residual meteorological variable data are the output from the NASA global atmospheric data assimilation system [38], as part of the Global Land Data Assimilation Systems [39]. The parameters utilized in this model are from the Goddard Earth Observing System Model Version 5 (GEOS-5) system [40]. The spin-up of the model is executed with Q2-based rainfall that is looped three times through three years of forcing data (2004–2006), which produces land-only model integrations. Studies such as those by Bowling *et al.* [41], Nijssen *et al.* [42], and Boone *et al.* [43] have demonstrated the ability of CLSM in depicting soil moisture dynamics. The consistency and high correlation (0.54) between CLSM simulated surface soil moisture data utilized in this research and *in situ* Oklahoma Mesonet observations have been demonstrated in [28].

### D. Data Matching

The Q2 radar-rainfall data set, which represents the reference rainfall in this study, is matched to the 2A12 overpass times and spatially averaged to the Catchment model grid resolution (25 km). The total number of overpasses and that of pixels considered in this study are 867 and 190 740, respectively. The Q2 pixels found within the land surface model pixel $A$ are utilized to compute the pixel-average reference rainfall rate

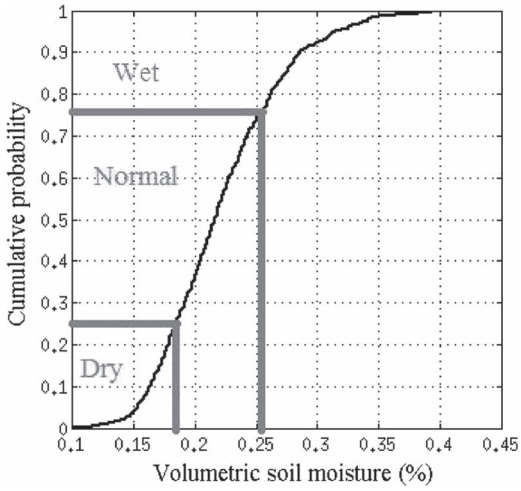


Fig. 3. Cumulative probability of the 2A12 orbit-average volumetric soil moisture for all 2A12 orbits in March to October of 2009 and 2010.

$R_{\mathrm{ref}}(A)$. The mean number of Q2 pixels (with the native Q2 resolution being 1 km$^2$) associated with a model grid cell is around 620. Matched estimates of 2A12 and $R_{\mathrm{ref}}(A)$ can only be produced at locations where actual observations were recorded by both the 2A12 and ground radars. On the other hand, the instantaneous satellite rainfall estimate $R_{\mathrm{sat}}(A)$ is a block-2A12 rainfall pixel computed to match each land surface model pixel. The average number of 2A12 pixels (with the native 2A12 resolution being around 8 km) associated with each model pixel is around 16. The 2A12 and Q2 data are dropped from comparison when there are more than 25% missing Q2 pixel values or when less than 8 2A12 pixels are

TABLE I
NUMBER OF SAMPLES ASSOCIATED WITH SOIL WETNESS CATEGORIES

| Soil Moisture Level | Number of overpasses | Number of pixels | Rainy pixels (%) | Pixels with rainfall > 8 mm/h (%) |
|---|---|---|---|---|
| **Wet** | 217 | 47740 | 16.70 | 3.65 |
| **Normal** | 434 | 95480 | 11.68 | 2.48 |
| **Dry** | 216 | 47520 | 9.30 | 1.04 |
| **Total** | 867 | 190740 | 12.34 | 2.61 |

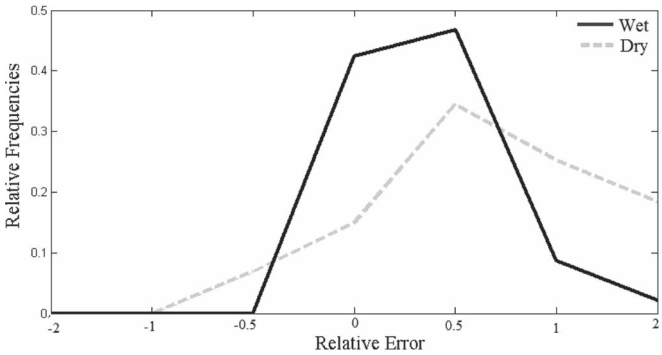


Fig. 4. Probability density function of relative error for all orbits.

available. By dropping these values, the block-Q2 values are more representative of the population that comprises the ground references, and the reliability of the block-2A12 values that comprise the satellite estimate is also increased. Statistics are applied on the matched Q2-2A12 data for comparing reference rainfall intensities to satellite-based estimates as a function of soil moisture conditions estimated by the Catchment model. Fig. 2 presents a sample of matched Q2 and 2A12 data for two representative cases of dry and wet surface conditions. In both cases, the spatial distribution of rainfall is similar between Q2 and 2A12, although the Q2 data capture greater rainfall intensity than 2A12. Fig. 2 represents a clear distinction between dry and wet conditions in terms of intensity and pattern.

The average soil moisture values from CLSM over the entire number of 2A12 overpasses are determined to provide the mean wetness condition over the area. Overpasses with more than 50 recorded values are considered for calculating mean soil moisture values, and therefore, 20% (254 overpasses) of the matched data were discarded from the error analysis. Fig. 3 shows the cumulative distribution of the area-average volumetric soil moisture values from CLSM over considered overpasses. The data from overpasses associated with area-average soil moisture of less than the 25th quantile represent dry conditions. Similarly, data from overpasses associated with area-average soil moisture higher than the 75th quantile represent wet conditions, whereas the remaining overpasses represent normal conditions. The number of overpasses and associated data sample statistics associated with each soil wetness category is presented in Table I. The rain fractions over the entire area and study period are 17%, 12%, and 9% for the wet, normal, and dry conditions, respectively. Fig. 4 shows the distribution of the satellite retrieval relative error (defined as the difference between 2A12 and Q2 values divided by the total for the detected rain values higher than 0.1 mm/h) computed at the pixel scale and instantaneous timescale for wet and dry conditions. It demonstrates a clear distinction in the probability density functions of satellite retrieval relative error under wet and dry conditions. Both distributions have their mode at 0.5 (overestimation of 2A12 compared to the reference), but the wet distribution is much narrower and more peaked than the dry distribution: The maximum relative frequency for the wet condition is 0.48 compared to 0.31 in dry conditions. The 2A12 rainfall retrievals present more random error over dry conditions. The greatest difference between wet and dry conditions can be seen around the zero relative error value. Overall, the systematic error of 2A12 retrieval is shown to be lower over wet versus dry land surface conditions.

## III. TMI RR ERROR ANALYSIS

In order to characterize the precipitation, additional Q2-based products are considered in this paper such as the freezing level height and the radar echo top. As brightness temperature channels associated with the ice scattering in precipitating clouds significantly influence the 2A12 retrievals over land, equivalent ice water content and a simplified rain-type classification were elaborated from the vertically integrated liquid content (VIL) provided at the original Q2 resolution (1 km, 5 min). The ice water content was evaluated from the 3-D reflectivity mosaics between the freezing level height and the echo top. A two-step approach similar to that by Steiner *et al.* [44] was applied to identify convective areas. First, the centers of convective cells are identified from the VIL map using a threshold value (5.5 $\mathrm{kg \cdot m^{-2}}$) above which it is assumed that precipitation can only result from convective processes. Then, an associated convective region is identified from surrounding pixels with VIL values greater than 2 $\mathrm{kg \cdot m^{-2}}$ at distances within 20 km. Pixels flagged as nonconvective are designated as stratiform.

For each common grid domain pixel $A$, a Convective Percent Index (CPI) is computed to quantify the contribution of convective rainfall to $R_{\mathrm{ref}}(A)$ as follows:

$$CPI(A) = 100 \frac{\sum_{j=1}^{nconv} Q2(a_j)}{\sum_{i=1}^{n} Q2(a_i)} \tag{1}$$

where $Q2$ denotes the Q2 RR at the original data product resolution (1 $\mathrm{km^2}$) $a_i$, $n$ is the number of Q2 data points inside the common grid pixel $A$, and $nconv \leq n$ is the number of Q2 pixels flagged as convective inside the pixel $A$. Each 2A12 pixel is associated with a rainfall rate at ground and with an associated convective rainfall rate. As for Q2, a CPI is computed to quantify the contribution of convective rainfall to $R(A)$. We also consider the inputs of the retrieval algorithm with the brightness temperatures from the 1B11 product

TABLE II
SAMPLES DEFINITION ACCORDING TO DIFFERENT CLASSES OF SOIL WETNESS AND VEGETATION INDEX

| | Dry<br>Soil wetness value < 0.178 | Medium | Wet<br>Soil wetness value > 0.309 |
|---|---|---|---|
| Low vegetation<br>NDVI < 0.411 | 2183 | 3357 | 2215 |
| Higher vegetation<br>NDVI > 0.411 | 5575 | 12158 | 5543 |

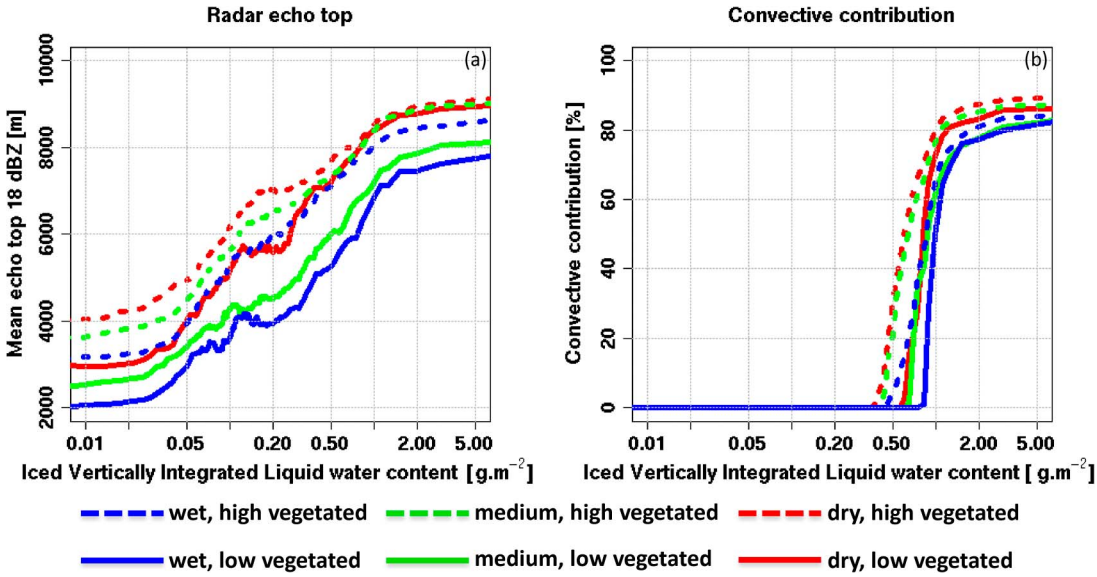


Fig. 5. (a) Averaged radar echo top and (b) convective volume contribution as functions of ice water content for various soil moisture and vegetation conditions.

measured by TMI. They are matched in space and time with the 2A12 products, the Q2 rainfall, and the soil moisture outputs from the land surface model. In order to preserve the statistical characteristics of the information input for the 2A12 algorithm, the brightness temperatures are taken at their native resolution.

For the last sample, we define two extreme surface wetness conditions (see Table II): "dry" that represents the 25% driest subsamples (soil wetness values below 0.178) and "wet" representing the 25% wettest subsamples (soil wetness values above 0.309). The vegetation was defined with two classes of the normalized difference vegetation index (NDVI) (see Table II): the low vegetated areas that represent the 25% subsamples with NDVI values below 0.411 and the remaining cases classified as "normal." These subsamples differ in terms of rainfall regimes. Fig. 5 shows the averaged echo top and the reference convective contribution of the sampled rainy systems as functions of the ice water content $VIL_{ice}$ over the six different surface conditions. All variables consistently increase with the $VIL_{ice}$ as a characterization of more intense convective systems ($VIL_{ice} > 0.3\ \mathrm{g \cdot m^{-2}}$) usually associated with high ice content.

The echo top and convective contribution $(CPI)$ values are higher over dry surfaces than over wet surfaces and higher over vegetated areas. The relation between these cloud features and surface characteristics is likely associated through a seasonal effect. During the warm season, more vegetation and drier soils are associated with higher convective activity related to thunderstorms. Wintertime period is associated with less vegetation, wetter soils, and lighter precipitation arising from large-scale frontal systems. The rain fraction increases with the $VIL_{ice}$ from less than 10% for $VIL_{ice} < 0.05\ \mathrm{g \cdot m^{-2}}$ up to more than 40% for $VIL_{ice} > 0.5\ \mathrm{g \cdot m^{-2}}$, and its values are generally higher over wet surfaces than over dry surfaces and lower over vegetated areas: Isolated convective cells are likely associated with dry and vegetated surfaces during the warm season, and more extended rain systems occur during the cold season over wet and less vegetated surfaces. The shifts of the RRs toward higher values over wet and less vegetated areas are correlated to the rain fraction. While higher RRs are generally associated with convective clouds, working at the 25-km resolution certainly explains why the differences of rain fraction are correlated to the differences of mean intensity over the various surfaces.

The features shown in Fig. 6 impact the brightness temperature (Tb) signatures of rain events from which the 2A12 algorithm infers RRs at the ground. Fig. 6 brings insight with the conditional median of the Tb distributions from 10V, 37V, and 85H channels over the various surfaces as functions of $VIL_{ice}$. Recall that the Tbs are taken at their native resolution. The distributions include Tb sampling raining and nonraining scenes because a given pixel is not necessary completely filled by rainfall (particularly for $VIL_{ice} < 0.2\ \mathrm{g \cdot m^{-2}}$; see Fig. 7). Differences at the lowest $VIL_{ice}$ values (associated

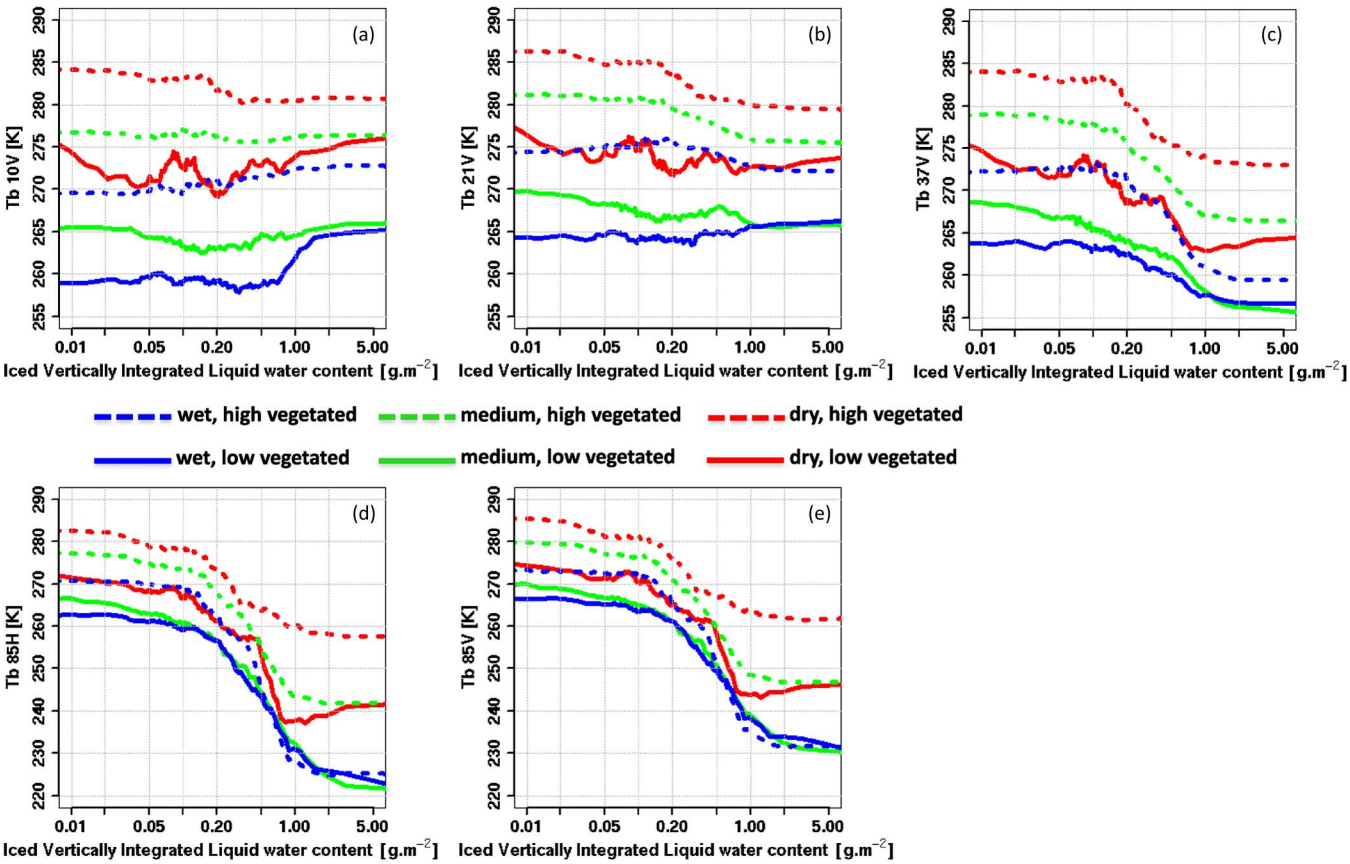


Fig. 6. Averaged brightness temperatures at (a) 10V, (b) 21V, (c) 37V, (d) 85H, and (e) 85V channels as functions of ice water content for various soil moisture and vegetation conditions.

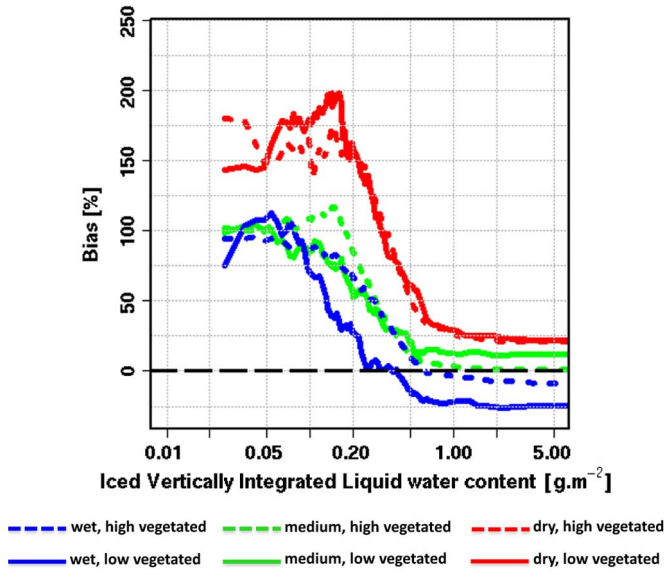


Fig. 7. Mean relative error of 2A12 versus reference as functions of ice water content for various soil moisture and vegetation conditions.

with light rain and rain/no-rain transition) could be linked to the differences in surface emissivity between the regions. For all channels considered, the Tb distributions are shifted toward lower values over wet surfaces compared to dry surfaces (e.g., ∼15 K Tb drop from dry to wet soil conditions at a 10-GHz channel over low vegetated areas) and downward over less vegetated areas (e.g., ∼10 K Tb drop for low vegetated areas at a 10-GHz channel). It is likely that the surface (soil moisture and vegetation) affects the lower frequency Tb (10- and 21-GHz channels) because the dielectric constant of water is higher than that of soil, so the surface emissivity (and upwelling Tb) is colder over a wet soil than a dry soil. The wintertime period associated with less vegetation is characterized by colder skin temperature that also decreases the upwelling Tb. Surface emissivity may have an impact at higher frequencies (85-GHz channel) when the rain fraction is low, particularly for $VIL_{ice} < 0.2$ g · m$^{-2}$. The higher frequency channels present consistently higher sensitivity to the $VIL_{ice}$. The surface is probably masked once precipitation develops an optically thick ice canopy at ∼0.3 g · m$^{-2}$. A difference of ice content, ice density, or spatial homogeneity of the ice field may drive the differences in Tb at the 85-GHz channel.

All of these characteristics present a significant diversity for assessing the 2A12 precipitation retrievals. Note that the seasonal cycle of the surface due to the time of the year is correlated to the seasonal cycle of precipitation characteristics. It is difficult to distinguish uniquely the impact of the surface conditions on the 2A12 retrievals from the impact of the vertical structure of the precipitating clouds.

To investigate the rainfall quantification from 2A12, Fig. 7 shows the behavior of the mean relative error (expressed in percentage) as a function of $VIL_{ice}$ for various conditions of soil moisture and vegetation. A rainy pixel is included in the statistics if both the satellite and reference are nonzero to emphasize the satellite sensor's ability to quantify precipitation

TABLE III
SREM2D CALIBRATION PARAMETERS FOR WET, NORMAL, DRY SOILS, AND UNCONDITIONAL

| | Dry | Normal | Wet | Unconditional |
|---|---|---|---|---|
| **POD** | Look Up table | | | |
| **Mean (mu-Gaussian of log-error)** | Look Up table | | | |
| **Sigma (std.dev Gaussian of log-error)** | 1.15 | 1.15 | 1.12 | 1.14 |
| **Non-detected mean rain rate (mm/hr)** | 0.10 | 0.13 | 0.14 | 0.12 |
| **$POD_{no\text{-}rain}$** | 0.93 | 0.97 | 0.97 | 0.97 |
| **$CL_{ret}$ (km)** | 65 | 34 | 66 | 53 |
| **$CL_{rain\ det}$ (km)** | 36 | 190 | 139 | 150 |
| **$CL_{no\ rain\ det}$ (km)** | 61 | 103 | 79 | 86 |

when it is raining. The satellite algorithm significantly overestimates the reference mean values for dry and medium soil moisture conditions over the range of ice water content values. For wet conditions, 2A12 overestimates the reference values for $VIL_{ice} < 0.3\ \mathrm{g \cdot m^{-2}}$ and underestimates the reference values for $VIL_{ice} > 1\ \mathrm{g \cdot m^{-2}}$. The degree of overestimation significantly relates to the soil moisture with greater MRE values (up to 250%) over dry surface conditions and lower MRE values (up to 150%) over wet surface conditions. One can note that the impact of the vegetation on the bias seems less important than that of soil moisture. The overestimation decreases with increasing $VIL_{ice}$ with the strongest decrease being at $VIL_{ice}$ below $1\ \mathrm{g \cdot m^{-2}}$. This pattern correlates well with the rapid drop of Tbs at 37V and 85H GHz channels (see Fig. 6).

The increase in the satellite-based overestimation of RRs from wet to dry soil moisture conditions is correlated with the corresponding increase in the overestimation of convective detection and convective fraction from the same range of wetness conditions (shown in Fig. 5). Because convective rainfall generally implies greater rainfall rates than stratiform rainfall (see [16, Figs. 1 and 3]), a weighting shifted toward positively biased convective fractions would result in the overestimation of 2A12 RRs. Therefore, this increase in the positive bias relative to the reference from wet to dry regions is attributed to the rainfall misclassification of the 2A12 algorithm.

## IV. RAINFALL ERROR MODELING (SREM2D)

SREM2D is a 2-D satellite rainfall error model developed for simulating satellite rainfall ensembles by perturbing a reference rainfall field [25], [26]. However, in this study, we run the model in inverse mode, which works in the opposite way; namely, we force the model with the "satellite" data set to obtain "reference"-like (i.e., error-corrected) rainfall ensembles. Specifically, SREM2D was forced here with Q2 radar estimates to produce 2A12 (satellite)-like rain fields. SREM2D can model both the spatial and the temporal variability of the satellite retrieval error as well as the spatial structure of the successful delineation of rainy and nonrainy areas. This aspect of SREM2D is innovative with respect to standard rainfall error models, which usually assume the perfect delineation of rain areas and simply scale the input precipitation forcing with a multiplicative perturbation [45]. Previous studies have demonstrated that rainfall ensembles produced by SREM2D provide better encapsulation of the reference radar precipitation and they better reproduce satellite rainfall error statistics (such as bias and root-mean-square error) than simpler rainfall error models [26], [28].

In this paper, we perturbed 2A12 satellite data through SREM2D to generate an ensemble of 50 Q2-like realizations. The input error parameters evaluated for 2A12 with respect to the high-quality Q2 product along the study period (i.e., the two warm periods of 2009 and 2010) are as follows: 1) probability of rain detection (POD); 2) mean of the logarithmic error (mu-Gaussian of log-error), defined as the log-error, where error is the multiplicative factor "e" as in $\mathrm{Rsensor} = \mathrm{Rreference} * \mathrm{e}$; 3) nondetected mean RR; 4) probability of no-rain detection $(\mathrm{POD_{no-rain}})$; 5) correlation length for the retrieval error $(\mathrm{CL_{ret}})$; 6) correlation length for the successful delineation of rain $(\mathrm{CL_{rain\ det}})$; and 7) correlation length for the successful delineation of no rain $(\mathrm{CL_{no\ rain\ det}})$. For more details about the model parameters, we refer the reader to [25].

SREM2D model parameters are determined based on two different approaches, hereafter named conditional and unconditional. In the conditional approach, the model parameters are computed for each area-average soil wetness category (defined in Section III) separately; in the unconditional approach, the model parameters are calibrated based on the entire matched database independent of soil wetness condition. The model parameters are summarized in Table III. Results indicate that SREM2D calibration parameters are different for the different wetness categories. In terms of spatial patterns, the correlation lengths of rain detection, no-rain detection, and retrieval error for the unconditional approach are less than 150 km and consistently fall between resulted values for wet and normal categories. The lower correlation length can be translated to the lower dependence between variables in space. Regarding the random error, the range of standard deviation of logarithmic multiplicative error is between 1.12 (wet) and 1.15 (dry) and equals 1.14 in the unconditional approach. The values represent the higher magnitude of error between the reference and sensor data in dry condition relative to the wet and unconditional approaches. The $\mathrm{POD_{no-rain}}$ for the unconditional approach is equal to 0.97, and it is the same when computed for wet and normal conditions, while for dry condition, it is slightly lower (0.93). The nondetected mean RR is 0.14 (0.10) in wet (dry) condition, whereas its value for the unconditional approach is 0.12. Wet conditions are related to higher RRs, which results in higher nondetected RRs from 2A12.

Furthermore, some SREM2D parameters are presented as a function of satellite RR thresholds (see Figs. 8 and 9). In fact,

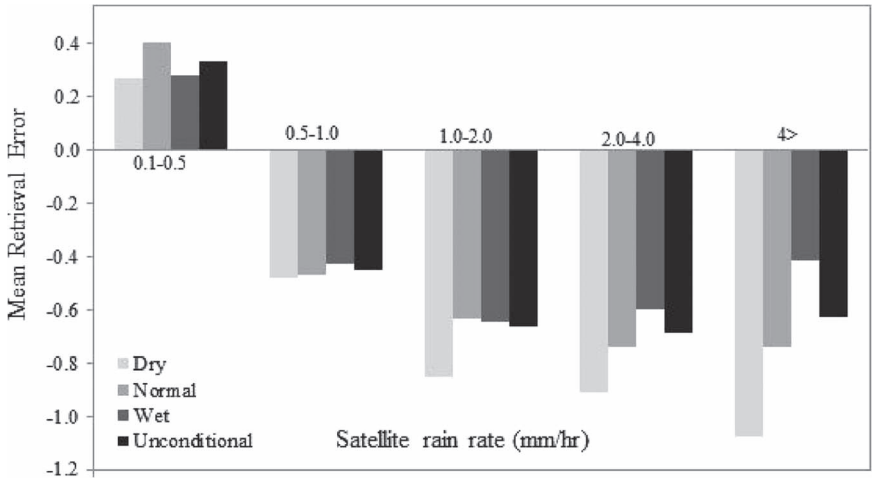


Fig. 8. Mean of 2A12 retrieval error versus rainfall threshold for wet, normal, dry soils, and unconditional approach.

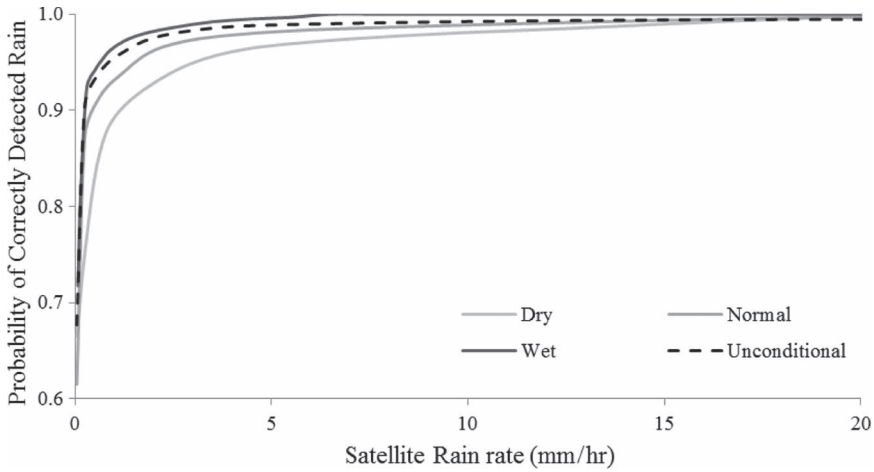


Fig. 9. Probability of correctly detected rain versus rainfall threshold for wet, normal, dry soils, and unconditional approach.

preliminary calculations indicated that parameters such as the POD and the mean error are functions of RR. For instance, the mean error shows positive values in low RRs and negative values in high RRs. This is consistent with the Kirstetter *et al.* [46] results demonstrated over West Africa for a similar overland PMW algorithm. In terms of POD, the dry surface soil moisture levels have the lowest values, whereas wet conditions have the highest POD values. The surface soil moisture levels in the unconditional approach converge at higher levels of satellite RR. Thus, a dynamic characterization of these error parameters is chosen in place of a single value, representing a novelty with respect to the original version of SREM2D.

After calibration, SREM2D is used to generate 50 rainfall ensembles from overpasses in each soil wetness category based on the two calibration approaches (conditional and unconditional). Fig. 10 shows the time series of cumulative rainfall simulated by SREM2D for each ensemble member using the two calibration approaches. The range of ensembles in the unconditional versus conditional SREM2D parameter calibration approach shows differences in the encapsulation of the actual rainfall time series. The conditional approach exhibits a much smaller ensemble range than the unconditional approach. Overall, Fig. 10 indicates better convergence of SREM2D ensemble members in the conditional approach.

## V. Results

The ensemble-based error modeling results are presented here for the two SREM2D calibration approaches, where parameters are conditioned or not to the simulated orbit-average soil moisture values. Specifically, in Section V-A, we provide error metrics (relative standard deviation and efficiency coefficient) to evaluate the improvement of conditional (surface moisture wetness) error modeling relative to unconditional error modeling, whereas in Section V-B, we perform an ensemble verification of the SREM2D rainfall ensembles produced using the different calibration approaches to further quantify the improvement due to the use of soil wetness information.

### A. Error Metrics

Two error metrics are presented in this section to evaluate the improvement of applying error modeling conditional to the near-surface soil moisture versus error modeling without the use of soil moisture information. The first error metric is the ratio of standard deviation (RSTD) of differences between SREM2D-generated ensemble mean values and Q2 rainfall values to the mean Q2 radar rainfall values, as in (2), shown at the bottom of the next page, where $R^i_{\mathrm{sat}_{\mathrm{mean}}}$ is the SREM2D-generated orbit-average satellite rainfall ensemble, $R^i_{\mathrm{ref}_{\mathrm{mean}}}$ is the

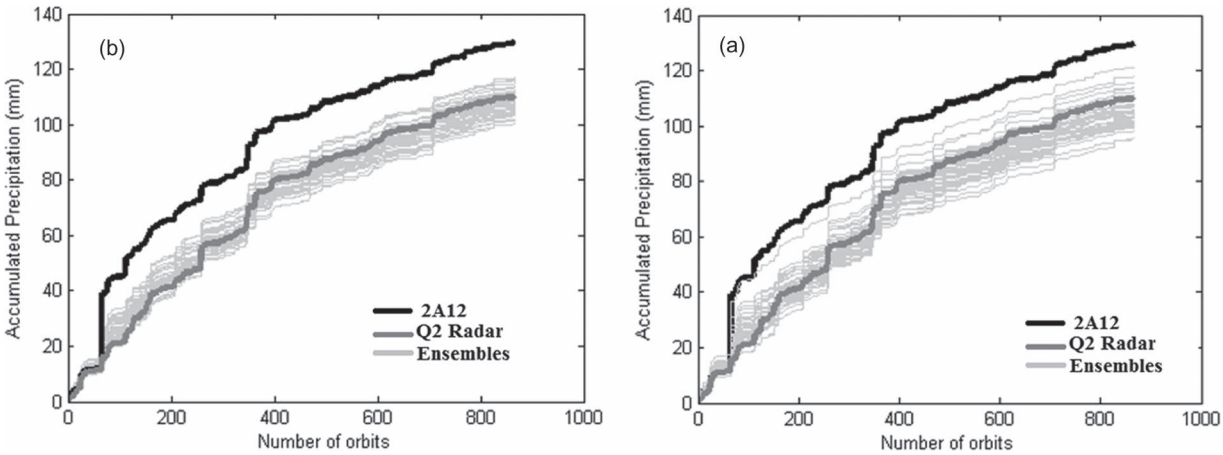


Fig. 10. Time series of cumulative rainfall of Q2, 2A12, and SREM2D ensemble members. In panel (a), SREM2D parameters are calibrated with the conditional approach, and in panel (b), SREM2D parameters are calibrated with the unconditional approach.

orbit-average reference radar rainfall, and $\bar{R}_{\mathrm{ref}_{\mathrm{mean}}}$ is the mean radar rainfall over all orbits. $U_j$ and $i$ represent the ensemble number and orbit number, respectively, while $N$ is the total number of orbits. The second error metric is the Nash–Sutcliffe efficiency [47], [48], which is presented to evaluate the goodness of fit of the SREM2D-generated ensembles and radar Q2 data

$$NSE(U_j) = 1 - \frac{\Sigma_1^N \left(R^i_{\mathrm{sat}_{\mathrm{mean}}}(U_j) - R^i_{\mathrm{ref}_{\mathrm{mean}}}\right)^2}{\Sigma_1^N \left(R^i_{\mathrm{ref}_{\mathrm{mean}}} - \bar{R}^i_{\mathrm{ref}_{\mathrm{mean}}}\right)^2}. \quad (3)$$

Nash-Sutcliffe efficiency equal to one indicates perfect model performance, while zero indicates model performance equal to climatology. Negative NSE values indicate that the model prediction introduces more error variability than the variability of the retrieved process. The two error metrics are computed for ensembles generated with the two different SREM2D calibration approaches, namely, calibrating the SREM2D parameters conditional and unconditional to the soil moisture.

The results for RSTD and NSE are shown in the box plots of Figs. 11 and 12, respectively. For the RSTD plots, we note that the wet category's unconditional "box and whisker" plot has a relatively large interquartile range (IQR) compared to the conditional plots. Both conditional and unconditional plots are skewed to the lower value, which means that the concentration of values is closer to the 25th percentile. The 25th percentile value is 1.55 (1.7) for the conditional (unconditional) approach. The overall range of RSTD values is much larger in the unconditional simulation compared to the conditional simulation. Both approaches under normal wetness conditions show similar IQRs, similar overall range, and symmetrical distributions. Given all similarities, the 25th percentile for the conditional simulation is 1.75 compared to 1.9 for the unconditional one. For dry condition, the IQR for the unconditional simulation is larger than the conditional simulation, which corresponds to higher statistical dispersion in the unconditional simulation. Both are skewed to the lower value, as the data are concentrated closer to the 25th percentile, which is 1.7 and 1.75 for conditional and unconditional calibrations, respectively. Overall, the IQRs of the conditional simulations are smaller than the unconditional ones, which is a good indicator of lower variability in the generated ensembles.

Similar to the RSTD error metric, under wet conditions, the unconditional error model ensemble exhibits a much larger IQR for the NSE values than the conditional error model ensemble. The 25th percentile is 0.28 for the conditional case and $-0.56$ for the unconditional one. Both cases are skewed to the higher end, meaning that values are concentrated around the 75th percentile. In normal wetness conditions, the IQRs are similar to each other. The 25th percentiles are 0.55 and 0.45 for the conditional and unconditional error model ensembles, respectively. The dry condition plots are both skewed to the higher value, but their IQRs are largely different. The IQR of the unconditional error model ensemble is much greater than the IQR of the conditional one. The 25th percentiles are 0.1 and 0.58 for the unconditional and conditional error model ensembles, respectively. Overall, the conditional simulations perform better than the unconditional one: This is evident in that the conditional plots have higher concentration of NSE values closer to 1, indicating that the SREM2D ensemble corrections bring satellite data closer to the reference (Q2 radar data).

### B. Ensemble Verification

We used three ensemble verification methods to assess the accuracy of the SREM2D-derived ensembles in terms of

$$RSTD(U_j) = \frac{\sqrt[2]{\Sigma_i^n \left(\left(R^i_{\mathrm{sat}_{\mathrm{mean}}}(U_j) - R^i_{\mathrm{ref}_{\mathrm{mean}}}\right) - \overline{\left(R^l_{\mathrm{sat}_{\mathrm{mean}}}(U_j) - R^l_{\mathrm{ref}_{\mathrm{mean}}}\right)}\right)^2}}{\bar{R}_{\mathrm{ref}_{\mathrm{mean}}}} \quad (2)$$

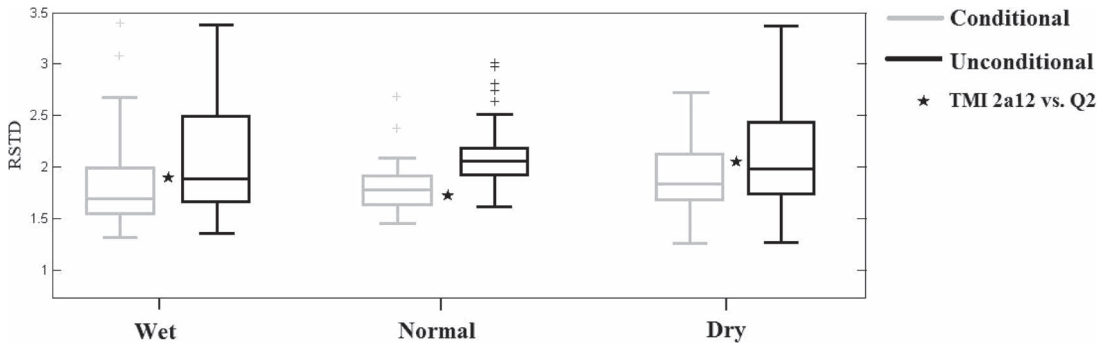


Fig. 11. Relative standard deviation (RSTD, unitless) of actual and SREM2D-generated ensemble members for 2A12 as function of wet, normal, and dry soil conditions.

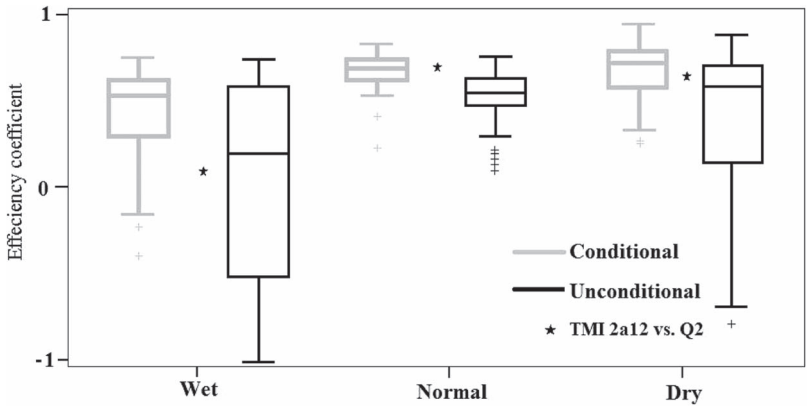


Fig. 12. Nash–Sutcliffe efficiency coefficient of actual and SREM2D-generated ensemble members for 2A12 in wet, normal, and dry soil conditions.

characterizing the variability of the satellite rainfall retrieval error: exceedance probability (EP), uncertainty ratio (UR), and rank histograms. The EP and UR have been suggested by previous studies as a way to evaluate probabilistic prediction performance [28], [49], [50]. These two metrics evaluate two contradictory aspects of error modeling: If the ensemble limits are too narrow, i.e., the EP is high, then the benchmark uncertainty is underestimated, while if the limits are too wide, i.e., the UR is high, the benchmark uncertainty is overestimated. In both cases, the model would have a poor predictive ability.

The EP is used to assess the ability of SREM2D-generated ensembles in encapsulating the reference data

$$EP = \frac{N_{exceedance}}{N_t} \tag{4}$$

where $N_{exceedance}$ is the number of times that the reference rainfall value falls outside the ensemble envelope and $N_t$ is the total number of data samples. A score of EP equal to zero indicates a perfect encapsulation of the reference within the ensemble envelope. On the other hand, if EP is equal to 1, that reference always falls outside the ensemble bounds. Results for EP values are shown in Fig. 13. The conditional simulation has a lower EP across all conditions. The difference between the resulted EP values of the conditional and unconditional error model ensembles is larger under dry soil condition (32%), which means that the number of times that Q2 falls outside the ensemble envelope is decreasing if the conditional

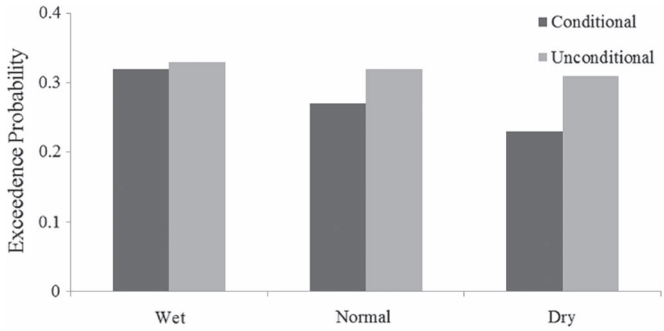


Fig. 13. EP of generated ensemble members of 2A12 in wet, normal, and dry soil conditions based on conditional and unconditional approaches.

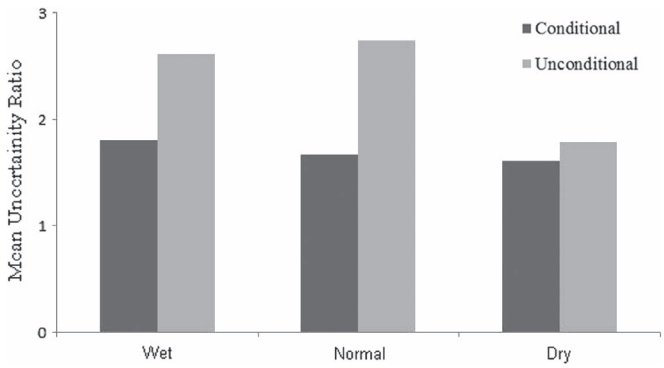


Fig. 14. Mean UR of generated ensembles of 2A12 rainfall for wet, normal, and dry soil conditions based on conditional and unconditional SREM2D parameter calibration.

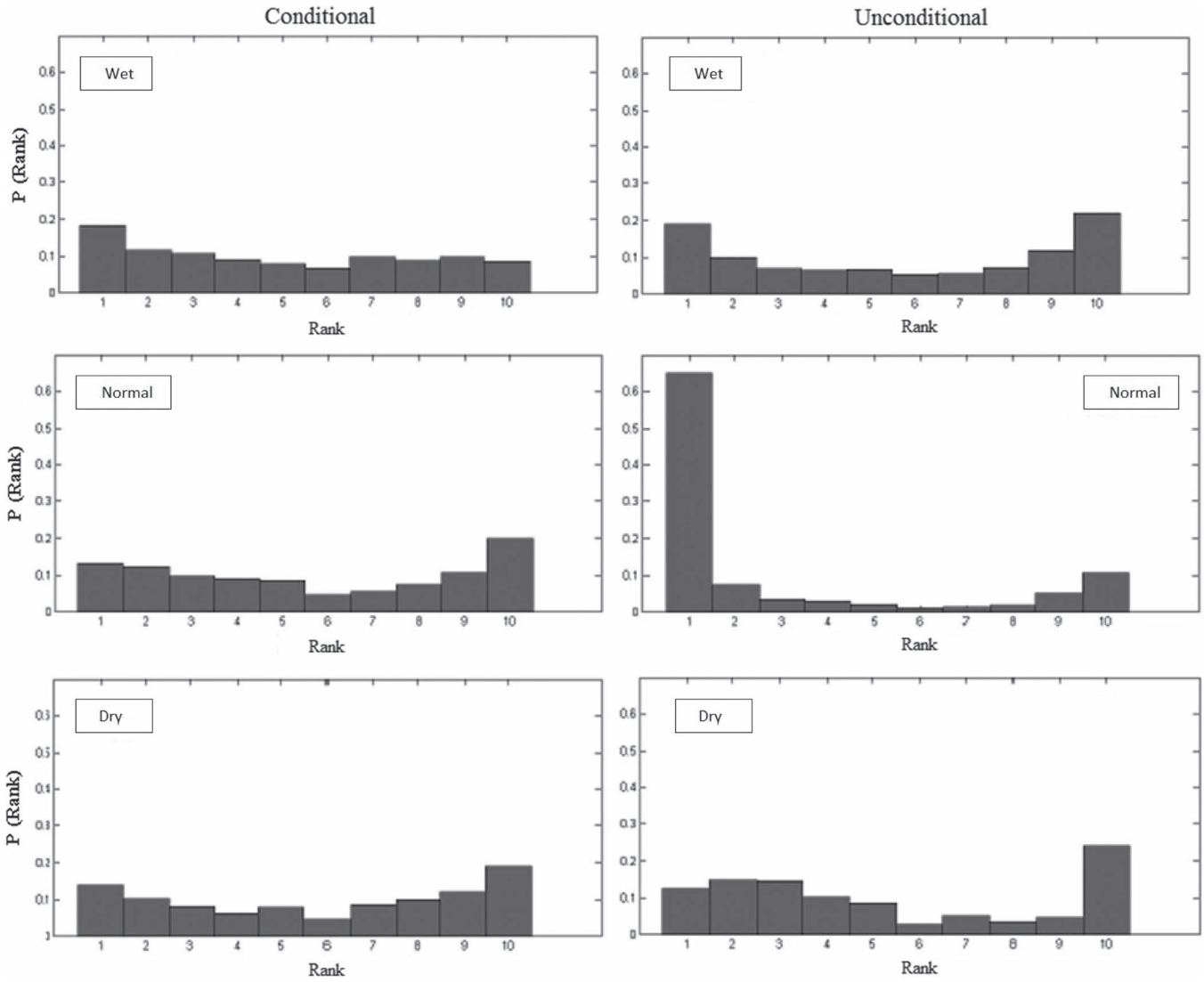


Fig. 15. Rank coefficient of generated ensemble members of 2A12 in (a) wet, (b) normal, and (c) dry soil conditions for conditional and unconditional approaches.

approach is applied. The unconditional and conditional results show the same trend: dry $>$ normal $>$ wet. The magnitude of improvement from unconditional to conditional increases also from dry to wet. Because the random error is greater for dry conditions (i.e., the spread is greater; see Fig. 4), it is harder for the reference rainfall to fall outside the ensemble envelope.

The mean UR is next used to evaluate the accuracy of ensemble envelope width. UR is computed as the ratio of aggregate ensemble widths divided by the "benchmark" uncertainty, defined as the difference between the ensemble mean and the reference rainfall

$$UR = \frac{\Sigma_1^N \left( R^i_{\mathrm{Sat}_{\mathrm{upper}}} - R^i_{\mathrm{Sat}_{\mathrm{lower}}} \right)}{2 \times \Sigma_1^N \left| \hat{R}^i_{\mathrm{sat}} - R^i_{\mathrm{ref}} \right|} \tag{5}$$

where $R^i_{\mathrm{Sat}_{\mathrm{upper}}}$ and $R^i_{\mathrm{Sat}_{\mathrm{lower}}}$ represent the upper and lower bounds of the simulated ensemble, respectively, $\hat{R}^i_{\mathrm{sat}}$ represents the mean of the generated ensemble over orbit number $i$, $R^i_{\mathrm{ref}}$ is the radar rainfall field over orbit number $i$, $i$ is the orbit number, and $N$ is the total number of orbits in each category. A UR value of 1 refers to a perfect delineation of Q2. A UR value greater than 1 corresponds to an overestimation of the actual uncertainty, whereas a UR value less than 1 means that the ensemble underestimates the benchmark uncertainty.

Fig. 14 shows the mean UR calculated for SREM2D ensembles generated by conditioning—or not—the parameters to the surface soil moisture. In all cases, the ensemble spread overestimated the actual error variability. Evidently, the ensemble generated with conditional parameters shows values of UR closer to 1, which corresponds to a better estimate of the actual uncertainty. The improvement is relatively higher in wet and normal soil wetness conditions.

Finally, rank histograms are used to evaluate the SREM2D ensemble predictions. If the model is able to correctly reproduce the prediction uncertainty, the ensemble members are equally likely to occur as in the reference simulation [51]. Namely, the number of times that the reference falls within any two adjacent ensemble members should be independent of

the position of the members in the ordered ensemble. Thus, the rank histogram, which is the histogram of the rate at which the reference falls into each interval, should be flat [52], [53]. Two shapes of the rank histogram, a U-shape and a sloped shape, are both indicators of poor ensemble predictions. Specifically, if a U-shaped histogram represents a lack of variability in the ensemble, a sloped histogram represents a constant bias in the ensemble prediction.

Results are shown in Fig. 15. For the unconditional approach (right panels), the U-shape rank histogram in the wet and normal conditions indicates that the ensemble suffered from the lack of variability, while the dry condition histogram exhibits an uneven pattern, which may result from the lack of variability and a bias in the ensemble prediction. Flatter rank histograms are observed for all ensembles obtained by conditioning the SREM2D parameters to the surface moisture level and can be interpreted as the equally likely occurrence of ensemble members as in the reference simulation.

## VI. Conclusion

In this paper, we assessed the impact of conditioning a stochastic error model for 2A12 rainfall estimates on near-surface soil moisture information derived from land surface simulations. The study used reference rainfall fields from the Q2 algorithm over Oklahoma for the warm season months of 2009 and 2010. TRMM orbit-average surface wetness conditions (wet, normal, and dry) over Oklahoma were defined based on surface soil moisture simulations from the NASA CLSM forced with Q2 rainfall fields. SREM2D, a 2-D satellite rainfall error model, was used to generate ensembles of satellite rainfall error with parameters that were conditioned or not to the three surface wetness conditions.

The error modeling improvement assessment was performed using different metrics: random error quantification (RSTD and NSE), uncertainty quantification (EP and UR), and ensemble verification (rank histograms). Significantly better performances in terms of all analyzed statistics are reported for the ensemble realizations generated using the conditional approach for estimating the SREM2D parameters. The IQR for the box plots of RSTD and NSE is larger for ensembles generated using the unconditional approach. This can be attributed to the statistical dispersion of ensemble realizations generated disregarding soil wetness conditions. The random ensemble error quantification exhibits lower EP and UR for the ensemble simulations conditioned to the soil wetness. This results in better encapsulation of the surface rainfall (represented by reference rainfall data) and more accurate estimation of the retrieval error variability on the basis of the SREM2D-generated ensembles.

The study relies upon the quality and specification of 2A12, Q2, and NASA CLSM simulations. Future studies should investigate ways to directly incorporate soil moisture as a parameter of the error model, as we demonstrated how some error statistics are highly dependent on it. As a first attempt to investigate this question, we focused on conditions ensuring good reference estimates. Performing the comparison during the warm season over Oklahoma offers the best measurement conditions related to VPR (i.e., radar beam below the melting layer) and beam blockage effects. Applying the same approach over various areas to assess the influence of other potential error factors (e.g., shallow convection over complex terrain) or during other seasons (with different soil moisture and vegetation conditions) will be the subject of future studies.

To generalize the findings of this study, it requires extending this error modeling exercise over different regions and longer periods of time and including additional surface characteristics (e.g., vegetation cover). The framework is applicable for the other microwave imagers on board low Earth orbiting satellites, and the result can be useful for the Global Precipitation Measurement mission.

## References

[1] F. J. Tapiador, F. J. Turk, W. Petersen, A. Y. Hou, E. García-Ortega, L. A. T. Machado, C. F. Angelis, P. Salioh, C. Kiddi, G. J. Huffman, and M. de Castro, "Global precipitation measurement: Methods, datasets and applications," *Atmos. Res.*, vol. 104/105, pp. 70–97, Feb. 2012.

[2] E. N. Anagnostou, C. A. Morales, and T. Dinku, "The use of TRMM precipitation radar observations in determining ground radar calibration biases," *J. Atmos. Ocean. Technol.*, vol. 18, no. 4, pp. 618–628, Apr. 2001.

[3] W. F. Krajewski, E. N. Anagnostou, and G. J. Ciach, "Effects of the radar observation process on inferred rainfall statistics," *J. Geophys. Res., Atmos.*, vol. 101, no. D21, pp. 26 493–26 502, Nov. 1996.

[4] W. F. Krajewski and J. A. Smith, "Radar hydrology: Rainfall estimation," *Adv. Water Resourc.*, vol. 25, no. 8–12, pp. 1387–1394, Aug.–Dec. 2002.

[5] R. A. Scofield and R. J. Kuligowski, "Status and outlook of operational satellite precipitation algorithms for extreme-precipitation events," *Weather Forecast.*, vol. 18, no. 6, pp. 1037–1051, Dec. 2003.

[6] E. E. Ebert and M. J. Manton, "Performance of satellite rainfall estimation algorithms during TOGA COARE," *J. Atmos. Sci.*, vol. 55, no. 9, pp. 1537–1557, May 1998.

[7] T. Heinemann and J. Kerényi, "The EUMETSAT multi sensor precipitation estimate (MPE): Concept and validation," presented at the EUMETSAT Users Conf., Weimar, Germany, 2003.

[8] J. Simpson, C. Kummerow, W. K. Tao, and R. F. Adler, "On the Tropical Rainfall Measuring Mission (TRMM)," *Meteorol. Atmos. Phys.*, vol. 60, no. 1–3, pp. 19–36, Mar. 1996.

[9] I. Lensky and V. Levizzani, "Estimation of precipitation from space-based platforms," in *Precipitation: Advances in Measurement, Estimation and Prediction*, S. Michaelides, Ed. Berlin, Germany: Springer-Verlag, 2008, pp. 195–217.

[10] C. Kummerow, H. Masunaga, and P. Bauer, "A next-generation microwave rainfall retrieval algorithm for use by TRMM and GPM," in *Measuring Precipitation From Space.*, V. Levizzani, P. Bauer, and F. J. Turk, Eds. Amsterdam, The Netherlands: Springer-Verlag, 2007, pp. 235–252.

[11] C. Kummerow, Y. Hong, W. S. Olson, S. Yang, R. F. Adler, J. McCollum, R. Ferraro, G. Petty, D.-B. Shina, and T. T. Wilheit, "The evolution of the Goddard Profiling algorithm (GPROF) for rainfall estimation from passive microwave sensors," *J. Appl. Meteorol.*, vol. 40, no. 11, pp. 1801–1820, Nov. 2001.

[12] N.-Y. Wang, C. Liu, R. Ferraro, D. Wolff, E. Zipser, and C. Kummerow, "TRMM 2A12 land precipitation product—Status and future plans," *J. Meteorol. Soc. Jpn. Ser. II*, vol. 87A, pp. 237–253, Mar. 2009.

[13] T. Dinku and E. N. Anagnostou, "Regional differences in overland rainfall estimation from PR-calibrated TMI algorithm," *J. Appl. Meteorol.*, vol. 44, no. 2, pp. 189–205, Feb. 2005.

[14] F. A. Furuzawa and K. Nakamura, "Differences of rainfall estimates over land by Tropical Rainfall Measuring Mission (TRMM) Precipitation Radar (PR) and TRMM Microwave Imager (TMI)—Dependence on storm height," *J. Appl. Meteorol.*, vol. 44, no. 3, pp. 367–383, Mar. 2005.

[15] J. R. McCollum and R. R. Ferraro, "Next generation of NOAA/NESDIS TMI, SSM/I, and AMSR-E microwave land rainfall algorithms," *J. Geophys. Res., Atmos.*, vol. 108, no. D8, pp. 8382–8404, Apr. 2003.

[16] K. Gopalan, N.-Y. Wang, R. Ferraro, and C. Liu, "Status of the TRMM 2A12 land precipitation algorithm," *J. Atmos. Ocean. Technol.*, vol. 27, no. 8, pp. 1343–1354, Aug. 2010.

[17] F. Aires, C. Prigent, F. Bernardo, C. Jiménez, R. Saunders, and P. Brunel, "A Tool to Estimate Land-Surface Emissivities at Microwave frequencies (TELSEM) for use in numerical weather prediction," *Q. J. R. Meteorol. Soc.*, vol. 137, no. 656, pp. 690–699, Apr. 2011.

[18] R. R. Ferraro, E. A. Smith, W. Berg, and G. J. Huffman, "A screening methodology for passive microwave precipitation retrieval algorithms," *J. Atmos. Sci.*, vol. 55, no. 9, pp. 1583–1600, May 1998.

[19] S. T. Fiorino and E. A. Smith, "Critical assessment of microphysical assumptions within TRMM radiometer rain profile algorithm using satellite, aircraft, and surface datasets from KWAJEX," *J. Appl. Meteorol. Climatol.*, vol. 45, no. 5, pp. 754–786, May 2006.

[20] C. Liu and E. J. Zipser, "'Warm Rain' in the tropics: Seasonal and regional distributions based on 9 yr of TRMM data," *J. Clim.*, vol. 22, no. 3, pp. 767–779, Feb. 2009.

[21] C. Liu, E. J. Zipser, D. J. Cecil, S. W. Nesbitt, and S. Sherwood, "A cloud and precipitation feature database from nine years of TRMM observations," *J. Appl. Meteorol. Climatol.*, vol. 47, no. 10, pp. 2712–2728, Oct. 2008.

[22] E. J. Zipser, C. Liu, D. J. Cecil, S. W. Nesbitt, and D. P. Yorty, "Where are the most intense thunderstorms on Earth?" *Bull. Amer. Meteorol. Soc.*, vol. 87, no. 8, pp. 1057–1071, Aug. 2006.

[23] S. Seto, N. Takahashi, and T. Iguchi, "Rain/no-rain classification methods for microwave radiometer observations over land using statistical information for brightness temperatures under no-rain conditions," *J. Appl. Meteorol.*, vol. 44, no. 8, pp. 1243–1259, Aug. 2005.

[24] P. E. Kirstetter, Y. Hong, J. J. Gourley, Q. Cao, M. Schwaller, W. Petersen, J. Zhang, E. Anagnostou, V. Maggioni, H. Seyyedi, and S. Chen, "Toward a research framework to bridge cross-platform error characterization of spaceborne passive/active sensors using NOAA/NSSL ground radar-based national mosaic QPE products over CONUS," presented at the Oral Presentation AGU Fall Meeting, San Francisco, CA, USA, 2012.

[25] F. Hossain and E. N. Anagnostou, "A two-dimensional satellite rainfall error model," *IEEE Trans. Geosci. Remote Sens.*, vol. 44, no. 6, pp. 1511–1522, Jun. 2006.

[26] F. Hossain and E. N. Anagnostou, "Assessment of a multidimensional satellite rainfall error model for ensemble generation of satellite rainfall data," *IEEE Geosci. Remote Sens. Lett.*, vol. 3, no. 3, pp. 419–423, Jul. 2006.

[27] V. Maggioni, E. N. Anagnostou, and R. H. Reichle, "The impact of model and rainfall forcing errors on characterizing soil moisture uncertainty in land surface modeling," *Hydrol. Earth Syst. Sci.*, vol. 16, no. 10, pp. 3499–3515, Oct. 2012.

[28] V. Maggioni, R. H. Reichle, and E. N. Anagnostou, "The effect of satellite rainfall error modeling on soil moisture prediction uncertainty," *J. Hydrometeorol.*, vol. 12, no. 3, pp. 413–428, Jun. 2011.

[29] J. Zhang, K. Howard, C. Langston, S. Vasiloff, B. Kaney, A. Arthur, S. Van Cooten, K. Kelleher, D. Kitzmiller, F. Ding, D.-J. Seo, E. Wells, and C. Dempsey, "National mosaic and multi-sensor QPE (NMQ) system: Description, results, and future plans," *Bull. Amer. Meteorol. Soc.*, vol. 92, no. 10, pp. 1321–1338, Oct. 2011.

[30] D. Kitzmiller, S. Van Cooten, F. Ding, K. Howard, C. Langston, J. Zhang, H. Moser, Y. Zhang, J. J. Gourley, D. Kim, and D. Riley, "Evolving multisensor precipitation estimation methods: Their impacts on flow prediction using a distributed hydrologic model," *J. Hydrometeorol.*, vol. 12, no. 6, pp. 1414–1431, Dec. 2011.

[31] V. Lakshmanan, A. Fritz, T. Smith, K. Hondl, and G. Stumpf, "An automated technique to quality control radar reflectivity data," *J. Appl. Meteorol. Climatol.*, vol. 46, no. 3, pp. 288–305, Mar. 2007.

[32] S. V. Vasiloff, K. W. Howard, R. M. Rabin, H. E. Brooks, D.-J. Seo, J. Zhang, D. H. Kitzmiller, M. G. Mullusky, W. F. Krajewski, E. A. Brandes, B. G. Brown, D. S. Berkowitz, J. A. McGinley, and R. J. Kuligowski, "Improving QPE and very short term QPF: An initiative for a community-wide integrated approach," *Bull. Amer. Meteorol. Soc.*, vol. 88, no. 12, pp. 1899–1911, Dec. 2007.

[33] J. Zhang, K. Howard, and J. J. Gourley, "Constructing three-dimensional multiple-radar reflectivity mosaics: Examples of convective storms and stratiform rain echoes," *J. Atmos. Ocean. Technol.*, vol. 22, no. 1, pp. 30–42, Jan. 2005.

[34] G. Villarini and W. F. Krajewski, "Sensitivity studies of the models of radar-rainfall uncertainties," *J. Appl. Meteorol. Climatol.*, vol. 49, no. 2, pp. 288–309, Feb. 2010.

[35] P.-E. Kirstetter, Y. Hong, J. J. Gourley, S. Chen, Z. Flamig, J. Zhang, M. Schwaller, W. Petersen, and E. Amitai, "Toward a framework for systematic error modeling of spaceborne precipitation radar with NOAA/NSSL ground radar-based national mosaic QPE," *J. Hydrometeorol.*, vol. 13, no. 4, pp. 1285–1300, Aug. 2012.

[36] A. Ducharne, R. D. Koster, M. J. Suarez, M. Stieglitz, and P. Kumar, "A catchment-based approach to modeling land surface processes in a general circulation model: 2. Parameter estimation and model demonstration," *J. Geophys. Res., Atmos.*, vol. 105, no. D20, pp. 24 823–24 838, Oct. 2000.

[37] R. D. Koster, M. J. Suarez, A. Ducharne, M. Stieglitz, and P. Kumar, "A catchment-based approach to modeling land surface processes in a general circulation model: 1. Model structure," *J. Geophys. Res., Atmos.*, vol. 105, no. D20, pp. 24 809–24 822, Oct. 2000.

[38] S. Bloom, A. da Silva, D. Dee, M. Bosilovich, J. D. Chern, S. Pawson, S. Schubert, M. Sienkiewicz, I. Stajner, W-W. Tan, and M-L. Wu, "Documentation and validation of the Goddard Earth Observing System (GEOS) data assimilation system, Version 4," NASA Goddard Space Flight Center, Greenbelt, MD, USA, Tech. Rep. NASA/TM-2005-104606 Vol. 26/Ver. 4, 2005.

[39] M. Rodell, P. R. Houser, U. Jambor, J. Gottschalck, K. Mitchell, C. J. Meng, K. Arsenault, B. Cosgrove, J. Radakovich, M. Bosilovich, J. K. Entin, J. P. Walker, D. Lohmann, and D. Toll, "The global land data assimilation system," *Bull. Amer. Meteorol. Soc.*, vol. 85, no. 3, pp. 381–394, Mar. 2004.

[40] M. M. Rienecker, M. J. Suarez, R. Todling, J. Bacmeister, L. Takacs, H.-C. Liu, W. Gu, M. Sienkiewicz, R. D. Koster, R. Gelaro, I. Stajner, and J. E. Nielsen, "The GEOS-5 data assimilation system-documentation of versions 5.0.1, 5.1.0, and 5.2.0," NASA Goddard Space Flight Center, Greenbelt, MD, USA, NASA/TM-2008-104606, 2008.

[41] L. C. Bowling, D. P. Lettenmaier, B. Nijssen, L. P. Graham, D. B. Clark, M. El Maayar, R. Essery, S. Goers, Y. M. Gusev, F. Habets, B. van den Hurk, J. Jin, D. Kahan, D. Lohmann, X. Ma, S. Mahanama, D. Mocko, O. Nasonova, G.-Y. Niu, P. Samuelsson, A. B. Shmakin, K. Takata, D. Verseghy, P. Viterbo, Y. Xia, Y. Xue, and Z.-L. Yang, "Simulation of high-latitude hydrological processes in the Torne–Kalix basin: PILPS Phase 2(e): 1: Experiment description and summary intercomparisons," *Glob. Planet. Change*, vol. 38, no. 1/2, pp. 1–30, Jul. 2003.

[42] B. Nijssen, L. C. Bowling, D. P. Lettenmaier, D. B. Clark, M. El Maayar, R. Essery, S. Goers, Y. M Gusev, F. Habets, B. van den Hurk, J. Jin, D. Kahan, D. Lohmann, X. Ma, S. Mahanama, D. Mocko, O. Nasonova, G.-Y. Niu, P. Samuelsson, A. B Shmakin, K. Takata, D. Verseghy, P. Viterbo, Y. Xia, Y. Xue, and Z.-L. Yang, "Simulation of high latitude hydrological processes in the Torne–Kalix basin: PILPS Phase 2(e): 2: Comparison of model results with observations," *Glob. Planet. Change*, vol. 38, no. 1/2, pp. 31–53, Jul. 2003.

[43] A. Boone, F. Habets, J. Noilhan, D. Clark, P. Dirmeyer, S. Fox, Y. Gusev, I. Haddeland, R. Koster, D. Lohmann, S. Mahanama, K. Mitchell, O. Nasonova, G.-Y. Niu, A. Pitman, J. Polcher, A. B. Shmakin, K. Tanaka, B. van den Hurk, S. Vérant, D. Verseghy, P. Viterbo, and Z.-L. Yang, "The Rhône-aggregation land surface scheme intercomparison project: An overview," *J. Clim.*, vol. 17, no. 1, pp. 187–208, Jan. 2004.

[44] M. Steiner, R. A. Houze, and S. E. Yuter, "Climatological characterization of three-dimensional storm structure from operational radar and rain gauge data," *J. Appl. Meteorol.*, vol. 34, no. 9, pp. 1978–2007, Sep. 1995.

[45] R. H. Reichle, R. D. Koster, P. Liu, S. P. P. Mahanama, E. G. Njoku, and M. Owe, "Comparison and assimilation of global soil moisture retrievals from the Advanced Microwave Scanning Radiometer for the Earth Observing System (AMSR-E) and the Scanning Multichannel Microwave Radiometer (SMMR)," *J. Geophys. Res., Atmos.*, vol. 112, no. D9, pp. D09108-1–D09108-14, May 2007.

[46] P.-E. Kirstetter, N. Viltard, and M. Gosset, "An error model for instantaneous satellite rainfall estimates: Evaluation of BRAIN-TMI over West Africa," *Q. J. R. Meteorol. Soc.*, vol. 139, no. 673, pp. 894–911, Apr. 2013.

[47] R. McCuen, Z. Knight, and A. Cutter, "Evaluation of the Nash–Sutcliffe efficiency index," *J. Hydrol. Eng.*, vol. 11, no. 6, pp. 597–602, Nov. 2006.

[48] J. E. Nash and J. V. Sutcliffe, "River flow forecasting through conceptual models part I—A discussion of principles," *J. Hydrol.*, vol. 10, no. 3, pp. 282–290, Apr. 1970.

[49] F. Hossain and E. N. Anagnostou, "Numerical investigation of the impact of uncertainties in satellite rainfall estimation and land surface model parameters on simulation of soil moisture," *Adv. Water Resourc.*, vol. 28, no. 12, pp. 1336–1350, Dec. 2005.

[50] F. Hossain, E. N. Anagnostou, T. Dinku, and M. Borga, "Hydrological model sensitivity to parameter and radar rainfall estimation uncertainty," *Hydrol. Process.*, vol. 18, no. 17, pp. 3277–3291, Dec. 2004.

[51] S. Siegert, J. Bröcker, and H. Kantz, "Rank histograms of stratified Monte Carlo ensembles," *Mon. Weather Rev.*, vol. 140, no. 5, pp. 1558–1571, May 2012.

[52] T. M. Hamill, "Interpretation of rank histograms for verifying ensemble forecasts," *Mon. Weather Rev.*, vol. 129, no. 3, pp. 550–560, Mar. 2001.

[53] T. M. Hamill and S. J. Colucci, "Verification of Eta–RSM short-range ensemble forecasts," *Mon. Weather Rev.*, vol. 125, no. 6, pp. 1312–1327, Jun. 1997.

**Hojjat Seyyedi** received the first M.S. degree in hydraulic structures from Shiraz University, Shiraz, Iran, in 2008 and the second M.S. degree in environmental modeling with focus on remote sensing and geographic information system from the University of Twente, Enschede, The Netherlands, in 2010. He has been working toward the Ph.D. degree in the Department of Civil and Environmental Engineering, University of Connecticut, Storrs, CT, USA, since 2010.

His research focuses on satellite meteorology, flood risk assessment, and catastrophe modeling. He has a six-year track record of working with different kinds of satellite and reanalysis precipitation measurements. During his M.S. study in the University of Twente, he evaluated the Multi sensor Precipitation Estimate products from METEOSAT8 and METEOSAT9 in comparison with ground-based radar data for the northwestern Europe. In his Ph.D. study, he succeeded to show the significance of near-surface soil moisture condition on microwave-based precipitation products. In addition, he assessed the error propagation from gridded precipitation data to simulated runoff through hydrological modeling. He also introduced a stochastic technique for error correction and spatial downscaling of global gridded precipitation products.

**Emmanouil N. Anagnostou** received the B.S degree in civil and environmental engineering from the National Technical University in Athens, Athens, Greece, in 1990 and the M.S and Ph.D. degrees in civil and environmental engineering from The University of Iowa, Iowa City, IA, USA, in 1995 and 1997, respectively.

He is currently a Professor of Civil and Environmental Engineering, the Northeast Utilities Endowed Chair in Environmental Engineering, and the Director of the Environmental Engineering Program at the University of Connecticut, Storrs, CT, USA. His primary research focuses on developing techniques for the remote sensing of precipitation from satellite sensors, ground-based weather radars, and underwater acoustic techniques. Other research interests include the integration of rainfall remote-sensing products in hydrologic modeling systems for the prediction of floods and developing weather-based damage prediction models for power distribution networks. He is the author or coauthor of more than 120 journal papers and several book chapters in the areas of precipitation remote sensing and hydrometeorological applications.

Dr. Anagnostou is a member of several international organizations and scientific committees.

**Pierre-Emmanuel Kirstetter** received the M.S. degree in civil engineering and environmental science from the Grenoble Institute of Technology, Saint-Martin-d'Hères, France, in 2004 and the M.S. degree in environmental sciences and the Ph.D. degree in hydrometeorology from Joseph Fourier University, Grenoble, France, in 2005 and 2008, respectively.

He is currently a Research Scientist at the NOAA National Severe Storm Laboratory and University of Oklahoma, Norman, OK, USA. His primary research focuses on the remote sensing of precipitation using satellite and ground-based weather radar. Consistency among sensors from field experiments and operational networks is evaluated from the microphysical up to the global scales. Other research interests include the assessment of uncertainties in quantitative precipitation estimation algorithms and their impact in hydrologic simulation. He is the author and coauthor of more than 30 papers and book chapters in the areas of precipitation remote sensing and hydrological applications.

Dr. Kirstetter is a member of international organizations and scientific committees such as the American Geophysical Union, NASA's Precipitation Measurement Missions science team, and the International Precipitation Working Group.

**Viviana Maggioni** received the B.S. and M.S. degrees in environmental engineering from the Politecnico di Milano, Milano, Italy, in 2003 and 2006, respectively, and the Ph.D. degree in environmental engineering from the University of Connecticut, Storrs, CT, USA, in 2012.

Since January 2014, she is an Assistant Professor of Civil and Environmental Engineering at George Mason University, Fairfax, VA, USA. Her research interests lie at the intersection of hydrometeorology and remote sensing, with a focus on satellite rainfall products and related uncertainty. She is also interested in the hydrological applicability of satellite rainfall observations in land data assimilation systems and in the error propagation from precipitation measurements to land surface simulations of soil moisture, runoff, and other hydrological variables.

**Yang Hong** received the B.S. degree in geosciences from the Peking University, Beijing, China, in 1996, the M.S. degree in environmental sciences from the Peking University, Beijing, China, in 1999, and the Ph.D. degree major in hydrology and water resources and the Ph.D. degree minor in remote sensing and spatial analysis from the University of Arizona, Tucson, AZ, USA, in 2003.

He is currently a Professor of hydrometeorology–climatology and remote sensing in the School of Civil Engineering and Environmental Sciences and in the School of Meteorology at the University of Oklahoma, Norman, OK, USA. Previously, he was a Research Scientist at NASA's Goddard Space Flight Center, Greenbelt, MD, USA, and a Postdoctoral Researcher at the University of California, Irvine, Irvine, CA, USA. He is currently the Director of the Hydrometeorology and Remote Sensing Laboratory (HyDROS Lab) at the National Weather Center, Norman OK, USA. His areas of research span the wide range of hydrology–meteorology–climatology, with particular interest in bridging the gap among the water–weather–climate–human systems across scales in space and time. He has developed and taught class topics such as remote-sensing retrieval and applications, advanced hydrologic modeling, climate change and natural hazards, engineering survey/measurement and statistics, land surface modeling and data assimilation systems for the hydrological cycle, and water systems under a changing climate.

Dr. Hong has served on several international and national committees, review panels, and the editorial board of several journals. He was the Chair of the American Geophysical Union Hydrology-Precipitation Technical Committee from 2008 to 2012. He was the recipient of the 2008 Group Achievement Award from the NASA Headquarters.

**Jonathan J. Gourley** received the B.S. and M.S. degrees in meteorology and the Ph.D. degree in civil engineering from the University of Oklahoma, Norman, OK, USA.

He is a Research Hydrologist with the NOAA/National Severe Storms Laboratory and an Affiliate Associate Professor with the School of Meteorology at the University of Oklahoma. His primary research interests include hydrologic prediction across scales ranging from water resources management down to the early warning of extreme events such as flash floods, and rainfall estimation from remote-sensing platforms such as satellite-based measurements and dual-polarization radar. He assembled a comprehensive database of flooding in the U.S. for community research purposes based on stream gauges, trained spotter reports, and witness reports collected directly from the public through an experiment that he coordinated. This database and others are being used to develop and evaluate a prototype modeling system called FLASH, which is being designed to provide state-of-the-art forecasts of flash flooding in real time over the U.S.

Dr. Gourley has won the Department of Commerce Bronze and Silver Medal Awards as well as the American Meteorological Society Journal of Hydrometeorology Editor's Award.